MAX-DOAS measurements of NO_2, SO_2, HCHO and BrO at the Mt. Waliguan WMO/GAW global baseline station in the Tibetan Plateau

Jianzhong Ma[1], Steffen Dörner[2], Sebastian Donner[2], Junli Jin[3], Siyang Cheng[1], Junrang Guo[1], Zhanfeng Zhang[4], Jianqiong Wang[4], Peng Liu[4], Guoqing Zhang[4], Janis Pukite[2], Johannes Lampel[5], Thomas Wagner[2]

[1]State Key Laboratory of Severe Weather & CMA Key Laboratory of Atmospheric Chemistry, Chinese Academy of Meteorological Sciences, Beijing, China

[2]Max Planck Institute for Chemistry, Mainz, Germany

[3]CMA Meteorological Observation Centre, Beijing, China

[4]Waliguan Observatory, Qinghai Meteorological Bureau, Xining, China

[5]Institute of Environmental Physics, University of Heidelberg, Heidelberg, Germany

Correspondence to: Thomas Wagner (thomas.wagner@mpic.de) and Jianzhong Ma (majz@cma.gov.cn)

Abstract.
Mt. Waliguan Observatory (WLG) is a World Meteorological Organization (WMO)/Global Atmosphere Watch (GAW) global baseline station in China. WLG is located at the northeastern part of the Tibetan plateau (36°17′N, 100°54′E, 3816 m a.s.l.) and is representative of the pristine atmosphere over the Eurasian continent. We made long-term ground-based MAX-DOAS measurements at WLG during the period 2012–2015. In this study, we retrieve the differential slant column densities (dSCDs) and estimate the tropospheric background mixing ratios of different trace gases, including NO_2, SO_2, HCHO and BrO, using the measured spectra at WLG. Averaging of 10 original spectra is found to be an ‘optimum option’ for reducing both the statistical error of the spectral retrieval and systematic errors in the analysis. The dSCDs of NO_2, SO_2, HCHO and BrO under clear sky and low aerosol load conditions are extracted from measured spectra at different elevation angles at WLG. By performing radiative transfer simulations with the model TRACY-2, we establish approximate relationships between the trace gas dSCDs at 1° elevation angle and the corresponding average tropospheric background volume mixing ratios. Mixing ratios of these trace gases in the lower troposphere over WLG are estimated to be in a range of about 5 ppt (January) to 70 ppt (May) for NO_2, below 0.5 ppb for SO_2, between 0.3 and 0.7 ppb for HCHO, and lower than 0.3 ppt for BrO. Our study provides valuable information and data set for further investigating tropospheric chemistry in the background atmosphere and their links to anthropogenic activities.

1 Introduction

Nitrogen oxides ($NO_x \equiv NO + NO_2$), sulfur dioxide (SO_2), formaldehyde (HCHO), and bromine monoxide (BrO) are important traces gases in tropospheric chemistry. Both NO_x and HCHO participate in the control of the strong oxidant O_3, which is an indicator of photochemical smog, and the strongest atmospheric oxidizing agent OH, which determines the lifetimes of many gaseous pollutants and greenhouse gases in the atmosphere (Seinfeld and Pandis, 2006;Ma et al., 2012;Lelieveld et al., 2016). NO_x and SO_2 are gaseous precursors of nitrate and sulfate aerosols, and large amounts of these aerosols can result in haze pollution and exert a strong negative radiative forcing on the climate change (Seinfeld and Pandis, 2006;Forster et al., 2007;Ma et al., 2010). NO_x and SO_2 are released from various anthropogenic emission sources, e.g., the burning of coal, oil, gas, wood, and straw (Granier et al., 2011;Zhao et al., 2012). NO_x is also emitted via natural processes including lightning and microbial activities in soils (Lee et al., 1997). Nitric oxide (NO) dominates NO_x released from these sources, but it can be quickly converted to nitrogen dioxide (NO_2) by reaction with ozone (O_3) in the atmosphere. Natural sources of SO_2 in the troposphere include volcanic eruptions and the atmospheric oxidation of dimethyl sulfide (DMS: CH_3SCH_3) emitted from the ocean (Dentener et al., 2006). HCHO in the remote atmosphere is produced through the oxidation of methane (CH_4) and non-methane volatile organic compounds (NMVOCs), and it is also emitted from anthropogenic combustion processes, biomass burning and natural vegetation (Stavrakou et al., 2009).

Global emissions and atmospheric abundance of gaseous pollutants (e.g., NO_x and SO_2) and aerosols have changed significantly over the past few decades as revealed predominantly by satellite observations (e.g., De Smedt et al., 2015;Xing et al., 2015;Bauwens et al., 2016;Fioletov et al., 2016;Krotkov et al., 2016;Klimont et al., 2017;Li et al., 2017;Georgoulias et al., 2018;Hammer et al., 2018;Ziemke et al., 2018). Worldwide ground-based monitoring the concentrations and trends of trace gases and aerosols in the atmosphere is essential for the validation of and filling gaps in satellite observations, in order to quantitatively assess the impacts of atmospheric composition change on global air quality and climate changes (Stohl et al., 2015;De Mazière et al., 2018). The international global measurement networks have been set up sequentially over the past decades to establish long-term databases for detecting changes and trends in the chemical and physical state of the atmosphere. Among the networks are the Global Atmosphere Watch (GAW) program of the World Meteorological Organization (WMO) and the Network for the Detection of Atmospheric Composition Change (NDACC), and in the latter measurements are performed mainly by ground-based remote-sensing techniques (De Mazière et al., 2018). In contrast to Europe and North America, the stations under the networks in Asia, especially in the remote areas, are very sparse.

The China Global Atmosphere Watch Baseline Observatory at Mt. Waliguan (WLG) is an in-land GAW baseline station affiliated to WMO. The site (3816 m a.s.l.), located at the northeastern part of the Tibetan plateau, is representative of the pristine atmosphere over the Eurasian continent. Air masses at WLG are highly representative of the remote free troposphere (Ma et al., 2002a). Previous model simulations constrained by measured mixing ratios of ozone and its precursors indicated a net destruction of ozone at WLG in the summertime of 1996 (Ma et al., 2002a). In contrast, new insights from model calculations based on more recent measurements showed that ozone was net produced by in situ photochemistry at WLG in late spring and summer of 2003 (Xue et al., 2013). The level of NO_x plays a key role in determining the sign of net ozone production in the remote troposphere. However, it is not determined if the difference in the estimated net ozone production at WLG between the two studies is caused by increasing NO_x from 1996 to 2003 or by the uncertainties in the measurements of NO_x. Similar to the earliest measurement of NO_2, SO_2, HCHO and other reactive gases were also measured by filter or canister sampling method at WLG at irregular time (Mu et al., 2007;Meng et al., 2010;Lin et al., 2013). It is necessary to start a new measurement program with advanced technique at WLG for the purpose of precisely monitoring the levels and trends of atmospheric composition in the global pristine atmosphere.

The multi-axis differential optical absorption spectroscopy (MAX-DOAS) has the potential to retrieve the vertical distributions of trace gases and aerosols in the immediate vicinity of the station from the scattered sunlight measured at multiple elevation angles (Hönninger and Platt, 2002;Bobrowski et al., 2003;Van Roozendael et al., 2003;Hönninger et al., 2004;Wittrock et al., 2004). As relatively simple and cheap ground-based instrumentation, the UV-visible MAX-DOAS will be included in the certified NDACC measurement technique for the observation of lower-tropospheric NO_2, HCHO and O_3 (De Mazière et al., 2018). Successful measurement and retrieval of trace gases (e.g., NO_2, SO_2 and HCHO) depend on various factors, including their molecular absorption features and atmospheric abundances as well as the atmospheric visibility and instrumental signal/noise ratio. In contrast to extensive ground-based measurements of NO_2, SO_2 and HCHO in rural and urban areas worldwide, including highly polluted areas in eastern China (e.g., Ma et al., 2013;Hendrick et al., 2014;Wang et al., 2014;Jin et al., 2016;Wang et al., 2017), measurements of these trace gases by MAX-DOAS in the remote background areas have been very sparse (Gomez et al., 2014;Gil-Ojeda et al., 2015;Schreier et al., 2016). Gomez et al. (2014) proposed a modified geometrical approach (MGA) to estimate long-path-averaged mixing ratios of trace gases from mountain MAX-DOAS measurements. A NO_2 level of 20 ppt, which is below the detection limit of the in situ instrumentation, was observed (Gomez et al., 2014). The MAX-DOAS technique has been applied to monitor the absolute column densities and plumes of SO_2 from large volcano eruptions (e.g., Lübcke et al., 2016;Tulet et al., 2017), but measuring SO_2 in the background free troposphere still remains challenging.

Bromine oxide (BrO) plays an import role in the catalytic destruction of ozone in the remote troposphere (Platt and Hönninger, 2003;von Glasow and Crutzen, 2007). The earliest MAX-DOAS measurements were focused on the retrieval of the mixing ratio levels and vertical profiles of BrO in the boundary layer of the Artic, salt lake and marine areas (Hönninger and Platt, 2002;Stutz et al., 2002;Leser et al., 2003;Frieß et al., 2004;Saiz-Lopez et al., 2004). Measurement results showed that the BrO mixing ratio could reach up to 30 ppt in the Actic and 10 ppt in the marine boundary layer (Platt and Hönninger, 2003;Martin et al., 2009). BrO in the free troposphere at the global scale was estimated to be at a level of 0.5–2 ppt based on space-borne, ground-based and sounding measurements by DOAS technique (Harder et al., 1998;Fitzenberger et al., 2000;Richter et al., 2002;Van Roozendael et al., 2002;Hendrick et al., 2007;Theys et al., 2007;Werner et al., 2017). Model calculations indicated that inorganic bromine can influence the chemical budgets of ozone in the free troposphere to a considerable extent, reducing O_3 concentration locally by up to 40% (von Glasow et al., 2004;Lary, 2005;Yang et al., 2005;Yang et al., 2010). Until now, measurements of BrO and related species by ground-based MAX-DOAS have been frequently carried out in the Arctic (Peterson et al., 2015;Peterson et al., 2017;Simpson et al., 2017;Luo et al., 2018), Antarctic (Wagner et al., 2007b;Roscoe et al., 2012;Prados-Roman et al., 2018) and coastal atmosphere (Coburn et al., 2011). To our knowledge, no MAX-DOAS measurements have been reported for BrO on continents other than polar, salt lake and coastal areas.

We made long-term ground-based MAX-DOAS measurements at WLG during the period 2012–2015. For this study we analyzed the measured spectra to retrieve the free tropospheric background mixing ratios of different trace gases, including NO_2, SO_2, HCHO and BrO, from MAX-DOAS measurements at WLG. Large effort was spent on the spectral analysis, because in spite of the rather long atmospheric light paths at high altitude the respective trace gas absorptions are close to or below the detection limit. In Sect. 2, we give a description of the WLG measurement site, the meteorological conditions, and the MAX-DOAS instrument used in the study. Sect. 3 describes the method and settings we used in the spectral retrieval. Sect. 4 introduces the radiative transfer simulations we performed for in-depth analysis of measurement data. Sect. 5 describes the methods to filter the measurement data for the clear sky and low aerosol load conditions. In Sect. 6, we provide the differential slant column density values of the investigated trace gases and their corresponding tropospheric background mixing ratios over WLG, and compare the levels of these trace gases reported by different studies. Conclusions are given in Sect. 7.

2 Field experiment

2.1 WLG station

The WLG station is sited at the top of Mt. Waliguan (36°17′N, 100°54′E, 3816 m a.s.l.), located in Qinghai Province of China (Fig. 1a). It is one of the WMO/GAW global baseline stations and only one in the hinterland of the Eurasian continent. Mt. Waliguan is an isolated mountain with an elevation of about 600 m relative to the surrounding landmass, being surrounded by highland steppes, tundra, deserts, and salt lakes (Fig. 1b). With a low population density of about 6 capitals km^{-2} and hardly any industry within 30 km, WLG has the advantage to be rather isolated from industry, forest and population centers. It is relatively dry, windy and short of precipitation with a typical continental plateau climate (Tang et al., 1995). Xining City (the capital of Qinghai Province, located about 90 km northeast of WLG) and Lanzhou City (the capital of Gansu Province, located about 260 km away to its east) are considered as the nearest large pollution sources that may have impacts on the WLG site. There are several high mountains (~4000 m a.s.l.) between Xining and Mt. Waliguan. Total column ozone, surface ozone, solar radiation, precipitation chemistry, greenhouse gases, aerosol optical depth, and aerosol scattering/absorption coefficient together with basic meteorological parameters have become operational measurement items at WLG in succession since the year 1991 (Tang et al., 1995). In addition to routine observations, intensive measurements and model analyses were performed to investigate the regional/global representativeness of WLG and the effects of chemical transformations, physical and transport processes on various atmospheric compositions, e.g., surface ozone, short-lifetime reactive gases (such as NO, NO_2, SO_2, CO, H_2O_2, HNO_3, HCHO, other carbonyls, and non-methane hydrocarbons (NMHCs)), greenhouse gases, persistent organic pollutants, metal and isotopes, and aerosols.

2.2 Meteorological conditions

We used the European Centre for Medium-Range Weather Forecasts (ECMWF) re-analysis data to investigate meteorological conditions over the WLG site, with data for 3-4 km altitude representing the ground level at WLG. As shown in Fig. S1, temperature is high in summer (around 283K) and low in winter (around 265K), pressure is high in summer (around 643 hPa) and low in winter (around 635 hPa), wind speed is low in summer (around 3m/s) and high in winter (around 5m/s), and wind direction (0 means the wind is blowing from the North) is from south-east in summer (around 140°) and from west in winter (around 260°). These seasonal variation characteristics are similar to those in earlier years at the station as reported in previous work (Tang et al., 1995). We evaluated the ECMWF reanalysis data for 3-4 km altitude using meteorological data from in situ measurements at the WLG station, and found that the ECMWF data are in good (temperature, pressure) and reasonable (wind speed and direction) agreement with in situ data (see Fig. S2).

2.3 MAX-DOAS instrument

We started the ground-based MAX-DOAS measurement program at WLG on 26 September 2010. An automated and compact (13 cm × 19 cm × 14 cm) Mini MAX-DOAS instrument from Hoffmann Messtechnik GmbH in Germany, which had ever been used at the Gucheng site in the North China Plain (Jin et al., 2016), was moved to and installed at WLG (Fig. 1c). This instrument is designed for the spectral analysis of scattered sunlight and the application of the MAX-DOAS technique (Hönninger et al., 2004). The same type of instrument was used in previous studies, e.g. in Beijing and the surrounding area (Ma et al., 2013;Jin et al., 2016). The entrance optics, fiber coupled spectrograph and controlling electronics are hermetically sealed in a metal box of about 3 liter volume. A stepper motor, mounted outside the box, can rotate the whole instrument to control the elevation viewing angle, i.e., the angle between the horizontal and the viewing direction, and thus it can scan vertically at different elevation angles. The spectrograph covers a wavelength range of 290-437 nm and its entrance slit has a width of 50 μm. A Sony ILX511 charged coupled device (CCD) detects the light in 2048 individual pixels. The whole spectrograph is cooled by a Peltier stage to maintain a stable temperature of the optical setup and to guarantee a small dark current signal. The measurement process and spectra data logging are controlled by a laptop using the MiniMAX software package developed by Dr. Udo Frieß at the Institute of Environmental Physics, the University of Heidelberg in Germany.

The instrument was mounted on a bracket, fixed at the building roof, at an azimuth viewing direction exactly towards the north. After a winter of pilot run, we added heating elements to the outside of the instrument so that the temperature of the spectrograph could be kept at a stable but not very low value, e.g., -10 °C in winter. In other seasons, the temperature of the optical setup was set at a higher value, typically of 0 °C, below the ambient temperature. Dark current spectra were measured using 10000 msec and 1 scan, and electronic offset spectra with 3 msec and 1000 scans. Measurements of these signal spectra were made generally month by month or whenever the working temperature of the instrument was changed. Over the pilot run period in the years 2010 and 2011, measurements had been made with the same sequence of elevation angles as used at the Gucheng site in the North China Plain (Jin et al., 2016), with no elevation angles lower than 3° available. After the beginning of the year 2012, the elevation angles were set to be -1°, 0°, 1°, 2°, 3°, 5°, 10°, 20°, 30°, and 90° in a sequence. Unfortunately, during the data analysis it turned out that the elevation calibration was wrong by -4° (see Fig. S3). Thus finally only a few elevation angles from the original selection were found to be above the horizon. After the correction by -4° the remaining elevation angles are: 1°, 6°, 16°, 26°, and 86°. The exposure time for each elevation angle was about one minute. The data from three years of measurements over the period April 2012 through April 2015 are used for this study.

3 Spectral retrieval

At the WLG site the atmospheric trace gas absorptions are usually rather low. Thus the settings of the spectral analysis were optimised for low detection limits. In general this can be achieved by

a) co-adding of individual spectra,
b) using rather broad spectral ranges,
c) selecting only spectra of high signal to noise ratio.

Since at the WLG station different detector temperatures were used for different time periods, the spectral analysis was performed with different spectral calibrations (and corresponding sets of convoluted cross sections) for each of these periods. Besides that, the spectral analysis was carried out with consistent settings for the different periods. In order to limit the amount of work, only ‘long periods’ that contained at least 60 measurement days were selected for the data analysis (see Table S1).

In order to achieve a large reduction of the statistical error, as much as possible individual spectra should be averaged. However, systematic errors tend to increase if an increasing number of spectra are averaged. In this study we performed the analysis of spectra averaged from 10 original spectra, for which a minimum of the fit error was found (see Fig. S4). In this study individual measurements at 26° elevation of each elevation sequence are used as Fraunhofer reference spectra, for the reasons explained in Supplement Sect. 3.2.

The spectral ranges for the retrieval of the different trace gases were determined in dedicated sensitivity studies (see Supplement Sect. 3.3). Examples of the spectral analyses are shown in Fig. 2. The errors of the retrieved differential slant column densities (dSCDs) of the trace gas were also estimated based on the sensitivity studies described in Supplement Sect. 3.3. Table 1 summarizes the spectral fitting ranges and systematic and random errors for the retrieved trace gas dSCDs. For all trace gases, the overall error for individual measurements (averages of 10 original spectra) is dominated by random errors. These errors, however, become much smaller if a large number of measurements are averaged.

4 Radiative transfer simulations

Similar to Gomez et al. (2014), we use the dSCDs from MAX-DOAS measurements to estimate the mixing ratios of NO_2, SO_2, HCHO, and BrO at WLG in this study. The relationships between the dSCDs and mixing ratios of these different trace gases are set up by radiative transfer simulations using the radiative transfer model TRACY-2 (Wagner et al., 2007a). This model allows to explicitly consider the variation of the topography around the measurement station. This option was, however, only used in one dimension (in viewing direction) in order to minimise the computational effort. The variation of the surface terrain height and the results of the radiative transfer simulations are illustrated in Fig. 3.

As a side aspect of our study, we also investigated the effect of different choices of the topography. In addition to the set-up with the 'true' topography (Fig. 3), we also performed simulations with flat surfaces at sea level or 3700m altitude. In all three set-ups the atmospheric properties and the altitude of the detector (3800m) are kept the same. In Fig. 4 the O_4 AMFs for the simulations with flat surfaces are plotted versus the O_4 AMFs for the true surface topography. While the results for a flat surface at 3700m are very similar to those for the true topography, the results for a flat surface at sea level show systematically higher values. With increasing aerosol load these differences even increase. In Fig. 5 the dependence of the simulated radiance (top) O_4 AMF (center) and colour index (bottom) are shown as function of the elevation angle (including negative elevation angles). Again, the results for the true topography and the flat surface at 3700m altitude are very similar, while the results for a flat surface at sea level are systematically different. The results of these comparisons indicate that the assumption of a flat surface at the approximate altitude of the surrounding terrain is a very good approximation for the true surface topography. Only for zero and negative elevation angles, the consideration of the true topography might become important.

The surface albedo was set to be 7.5%. Sensitivity studies indicated that the exact choice is not critical: Simulations with high surface albedo representative for snow surfaces yielded almost the same results. This finding can be understood by the fact that the measurements and the Fraunhofer reference spectra are affected by changes of the surface albedo in the same way. Thus, for the retrieved dSCDs the effect of the surface albedo cancels out. The aerosol extinction was varied, but was assumed to be constant between 2600 and 5600m altitude. Different aerosol loads (AOD between 0 and 0.5) were assumed. Here it should be noted that only a fraction of 60% of the total AOD is located above the instrument.

Simulations of trace gas air mass factors (AMFs) were performed for specific viewing geometries for a whole diurnal cycle in January and July. These months were chosen, because they represent the most extreme viewing geometries (winter and summer) during the whole year. From the derived diurnal variations of the trace gas AMFs, daily averages for measurements with SZA below 65 ° were calculated. For these calculations the individual AMFs were weighted by the corresponding simulated intensities. Finally, the simulated AMFs for 26 ° elevation angle were subtracted from the AMFs for the lower elevation angles yielding the respective differential AMFs (dAMFs). This procedure was applied in order to calculate trace gas dAMFs which can be directly compared to the trace gas dSCDs derived from the measurements.

In order to relate the measured trace gas dSCDs to atmospheric trace gas mixing ratios, assumptions about the vertical distributions of the trace gases have to be made. The assumed trace gas profiles are described in Supplement Sect. 4. Two types of input profiles are used: For the first group of trace gases, the influence of the stratospheric absorptions can be neglected. This is the case for SO_2 and HCHO, for which the stratospheric amounts (except for strong volcanic eruptions) are very small and can be neglected. Although for NO_2, the contribution from the stratospheric absorption can be rather large, it is found that the stratospheric NO_2 absorptions are very similar for the different elevation angles (see Supplement Sect. 5.1), and the stratospheric absorptions almost completely cancel out for the derived trace gas dSCDs using sequential Fraunhofer reference spectra. Thus, the tropospheric partial dSCD can be simulated independently from the stratospheric absorptions and can be directly compared to the measured NO_2 dSCDs.

For BrO, the situation is different: since the stratospheric BrO profile is located at rather low altitudes, the corresponding absorptions depend substantially on the elevation angle. Thus they don't cancel out in the retrieved BrO dSCDs. In fact, the dSCDs for low elevation angles even can become negative (see Supplement Sect. 5.2) due to the stratospheric BrO absorptions. Therefore, for BrO the stratospheric and tropospheric profiles of BrO have always to be considered simultaneously in the radiative transfer simulations.

From the simulations results for 1 ° elevation angle (and low aerosol load: AOD = 0.1) approximate relationships between the trace gas dSCDs (at 1 ° elevation angle) and the corresponding volume mixing ratios are derived. They are given below for the different trace gases:

SO_2: a dSCD of 1×10^{15} molec/cm² corresponds to a mixing ratio of 60 ppt,

NO_2: a dSCD of 1×10^{15} molec/cm² corresponds to a mixing ratio of 23 ppt,

HCHO: a dSCD of 1×10^{15} molec/cm² corresponds to a mixing ratio of 42 ppt,

BrO: a dSCD of 1×10^{13} molec/cm² corresponds to a mixing ratio of 0.6 ppt.

Here it should be noted that for BrO the relationship is valid for the increase of the BrO dSCD compared to a scenario with no BrO in the troposphere (see Supplement Sect. 5.2 and Fig. S23). It should also be noted that while in the simulations a constant mixing ratio throughout the atmosphere was assumed, the measured trace gas dSCDs are mainly sensitive to the trace gas concentrations in the atmospheric layers close to the instrument. Thus the derived trace gas mixing ratios are most representative for the free troposphere in the altitude range between about 4 and 5 km.

5 Identification of measurements made under cloudy sky conditions and high aerosol loads

For the quantitative interpretation of the measurements, they are compared to results from radiative transfer simulations. These simulations are performed for well defined, in particular cloud-free conditions. Thus only measurements for such conditions have to be selected. Moreover, to make benefit of the high sensitivity of the MAX-DOAS measurements, situations with low aerosol load and thus high visibility have to be selected. The following two sub-sections describe how measurements under cloudy conditions and high aerosol loads are identified.

5.1 Cloud filter

Cloudy sky conditions can be identified and classified by different quantities (see e.g. Gielen et al., 2014;Wagner et al., 2014;Wagner et al., 2016). In this study, to minimise the computational effort, we only use the colour index (CI) measured in zenith direction (note that the measurements in zenith direction were not used for trace gas retrievals because of suspected direct sun impact). We chose the wavelength pair 330 nm and 390 nm:

$$CI = \frac{signal(330\,nm)}{signal(390\,nm)} \quad (1)$$

Moreover, in order to minimise the potential effects of instrument degradation, not the absolute value of the CI is used for the cloud classification. Instead, two derived quantities are calculated:

1) The temporal smoothness indicator (TSI)

The TSI is derived from the zenith measurements. If the CI between subsequent zenith measurements changes rapidly, this indicates the presence of clouds. The TSI is calculated according to the following formula:

$$TSI_i = \left| \frac{CI_{i-1} - CI_{i+1}}{2} - CI_i \right| \quad (2)$$

Here i indicates the number of an elevation sequence. For clear sky (and homogenous cloud cover) the TSI is small. For broken clouds the TSI is large.

2) The spread (SP) of the CI for one elevation sequence

The SP is calculated as the difference between the maximum and minimum of the CI for a selected elevation sequence:

$$SP_i = \max(CI_i) - \min(CI_i) \quad (3)$$

Here $\max(CI_i)$ and $\min(CI_i)$ indicate the maximum and minimum CI of the considered elevation sequence. For clear sky, the SP is large, for (homogenous) clouds the SP is low.

Based on the calculated TSI and SP the cloud situation of an individual elevation sequence is classified as clear sky, broken clouds or continuous clouds according to the following thresholds:

a) Clear sky: TSI < 0.012 and SP > 0.15,
b) Broken clouds: TSI > 0.012,
c) Continuous clouds: TSI < 0.012 and SP < 0.15.

Note: for cases a) and c) both TSI (at the beginning and the end of the elevation sequence) have to be < 0.012); for case b) the condition is fulfilled if one of both TSI is > 0.012.

5.2 Aerosol filter

For the low elevation angles the atmospheric visibility and thus the length of the light path depends strongly on the aerosol load. Thus measurements with high aerosol loads have decreased sensitivity to the trace gas absorptions and have thus to be identified and removed from further processing. For that purpose the retrieved O_4 absorption is used (Wagner et al., 2004;Lampel et al., 2018). In the following a threshold for the retrieved O_4 dSCD at 1° elevation angle of 1.4×10^{43} molec^2/cm^5 is used, which corresponds to an O_4 dAMF of 1.2 (see Fig. S26). This threshold represents an AOD of about 0.1 at 360 nm.

In Fig. S27 the seasonal variation of the O_4 dSCDs at 1° elevation is shown. High values are typically found in winter indicating low AOD. In other seasons smaller O_4 dSCDs are found indicating higher AOD. This seasonal dependence is in good agreement with measurements of the AOD (Che et al., 2011).

5.3 Summary of sky conditions

In Fig. 6 the seasonal variation of the sky conditions is shown. It is derived by applying the cloud and aerosol classification algorithms described above. The statistics is based on the number of observations (at 1°, 6°, or 16° elevation angle) of spectra averaged from 10 original spectra (April 2012 – April 2015). Only measurements with more than 800 scans are considered. The basic colours indicate the cloud properties (clear, broken clouds, continuous clouds). The full or light colours indicate observations with low or high aerosol loads, respectively.

While the absolute frequency of clear sky observations (low and high aerosol load) stays almost constant over the year, the relative fraction changes strongly with the highest probability of clear sky observations in winter and the lowest probability in summer. The relative fraction of low aerosol cases is largest in winter. The corresponding seasonal frequency plots for the different trace gas analyses (after application of the individual RMS filters) are shown in Fig. S28. While the absolute amount of valid data is different for the different analyses, the seasonal frequency is almost the same.

6 Results

6.1 Seasonal means of the dSCDs

In Fig. 7 (left) time series of daily averages of the individual trace gas dSCDs for 1° elevation angle are shown. On the right side, the corresponding monthly mean values are shown. In Fig. 8 the seasonal cycles for all elevation angles (1°, 6°, 16°) are shown for clear sky. In this figure, also the systematic uncertainties of the trace gas dSCDs are indicated by the blue dotted lines. The systematic uncertainties can be regarded as indicators for the lower bounds of the detection limit (which might be reached if a large amount of measurements is averaged). For NO_2, SO_2, and HCHO, also approximate mixing ratios derived for the measurements at 1° elevation angles are indicated by the y-axes at the right side (see Sect. 4). The results for broken clouds are similar to those for clear sky (see Fig. S29). This is a useful information to confirm the results for clear sky, since for broken clouds, the atmospheric light paths are often similar to those for clear sky.

The main findings are:

i) For NO_2 and HCHO higher dSCDs are found for lower elevation angles, and this indicates enhanced trace gas mixing ratios in the troposphere (at least in the atmospheric layers between about 4 and 5km);

ii) the highest NO_2 values are found in a period from April to June, most likely due to the influence of long range transport of NO_2 and its reservoir from both human and natural sources (Ma et al., 2002b;Wang et al., 2006)

iii) for BrO the opposite dependence is found, and this is mainly caused by the influence of stratospheric BrO (see Supplement Sect. 5.2);

iv) for SO_2 no clear elevation dependence is found (the values are below detection limit).

6.2 Estimation of a free tropospheric background mixing ratio from the dSCDs

In this section the lower tropospheric mixing ratios of the NO_2, SO_2, HCHO, and BrO at WLG are estimated based on the respective dSCDs at 1 °(see Fig. 8) and the relationships between the dSCDs and the tropospheric mixing ratios (Sect. 4).

Below are our estimates:

NO_2: dSCDs at 1 ° between 0.2×10^{15} molec/cm ² (January) and 3×10^{15} molec/cm ² (May) correspond to mixing ratios between about 5 (January) and 70 ppt (May).

SO_2: dSCDs at 1 °below 8×10^{15} molec/cm ²correspond to mixing ratios below 0.5 ppb,

HCHO: dSCDs at 1 °between 0.7×10^{15} molec/cm ²(winter) and 1.7×10^{15} molec/cm ²(summer) correspond to mixing ratios between about 0.3 (winter) and 0.7 ppb (summer),

BrO: from the dSCDs at 1 °an upper limit for a troposphere BrO mixing ratio 0.3 ppt is derived (see Supplement Sect. 8).

It should again be noted that while in the simulations a constant mixing ratio throughout the atmosphere was assumed, the measured trace gas dSCDs are mainly sensitive to the trace gas concentrations in the atmospheric layers close to the instrument. Thus the derived trace gas mixing ratios are most representative for the free troposphere in the altitude range between about 4 and 5 km.

6.3 Comparisons with previous studies

Measurements of the very reactive trace gases are very scarce at remote sites like WLG. Table 2 summaries the mixing ratios of NO_2, SO_2, HCHO and BrO at WLG measured by MAX-DOAS presented in this study in comparison to those recorded in other studies using different methods.

The passive sampling method was used to measure the weekly and monthly mean mixing ratios of NO_2 and SO_2 at WLG (Ma et al., 2002a;Meng et al., 2010;Lin et al., 2013). The monthly mean mixing ratios and standard deviations of NO_2 at WLG were 0.022±0.010 ppb in January and 48±17 ppt in July for the year 1996 (Ma et al., 2002a). For the measurement in 1996, the NO_2 was sampled with filter packs (SP) with exposure times of typically 3–5 days, and then analyzed by ion chromatography equipment (ICG) (Yu et al., 1997). During the measurement experiment in 2008, the samplers were exposed about 10 days in a month. The extracted NO_2 samples (Ogawa Passive Samplers) were analyzed using a spectrophotometer (SPM) while the extracted SO_2 samples were analyzed by ICG (Meng et al., 2010). The average mixing ratios of NO_2 and SO_2 at WLG in 2008 varied typically in the ranges of 0.6±0.4 ppb and 0.7±0.4 ppb, respectively (Meng et al., 2010). Long-term continuous measurements, by filter sampling with exposure times of 3-5 days followed by ICG chemical analysis, showed that the mixing ratio of SO_2 varied typically in a range of 0.45±0.14 ppb at WLG from 1997 to 2009 (Lin et al., 2013). The NO_2 levels obtained from this study are in accordance with those recorded by Ma et al. (2002a), but an order of magnitude lower than reported by Meng et al. (2010). The time differences between Meng et al. (2010) and the other two studies seems not to be the main cause. The sampling filters were likely to be polluted by local human activities, such as increasing frequency of occasional cars and vans to the station, which could not be excluded from the recording due to their long exposure time. The level of SO_2 might also be overestimated by Meng et al. (2010) considering that there had not been a significant increasing trend for SO_2 at WLG during 1997-2009 (Lin et al., 2013). It can be deduced that the SO_2 level from this study is reasonable with comparison to the results from Lin et al. (2013).

The daytime NO and NO_2 mixing ratios at WLG in the summer of 2006 were 71±45 ppt and 0.28±0.13 ppb, respectively, as measured by chemiluminescence analyzer (CLS) coupled with a photolytic converter (PhC) (Xue et al., 2011). Also measured by CLS, the daytime average NO mixing ratios at WLG were 0.072±0.079 ppb in the late spring and 0.047±0.032

ppb in the summer of 2003 (Wang et al., 2006;Xue et al., 2013). Assuming the same NO_2/NO ratio (i.e., 3.9) as in the summer of 2006, the NO_2 mixing ratios at WLG would be 0.28 ±0.31 ppb in the late spring and 0.18 ±0.12 ppb in the summer of 2003. The NO_2 levels obtained from the CLS method are much higher than those from MAX-DOAS presented in this study. This can be explained by two facts: (1) There are systematic biases in the NO_2 mixing ratios derived by the CLS/PhC method due to the interferences from other oxidation products, such as nitric acid and organic nitrate, which are accounted as NO_2; (2) In situ measurements at WLG are strongly influenced during the daytime by the underlying boundary layer, where NO_2 levels are high due to soil emissions and other occasional pollution sources. In contrast, the upwelling air masses have a relative small influence on the MAXDOAS measurements, which represent a long optical path.

The ambient concentrations of carbonyl compounds were measured at WLG in 2005, by using the silica gel cartridge/high-performance liquid chromatography (SGC/HPLC) method. The means and standard deviations of HCHO mixing ratios were 4.16 ±1.89 ppb in August-September and 1.48 ±0.42 ppb in December (Mu et al., 2007). The HCHO mixing ratios obtained by the SGC/HPLC method are nearly an order of magnitude higher than those by MAX-DOAS presented in this study. Mu et al. (2007) reported that the variability of HCHO concentrations was significant (by a factor of >2) if the air samples were collected at different places at the site. However, this cannot fully explain the large difference in the HCHO level at WLG between the two studies. Since HCHO forms through various oxidation reactions associated with volatile organics, the results from HPLC might not be well representative of air conditions under which the air samples had been collected some days ago.

Also listed in Table 2 are the levels of NO_2, HCHO and BrO measured by MAX-DOAS in other remote areas at middle and subtropical latitudes. Note that to our knowledge, no results for SO_2 were reported in those studies. Our purpose here is to show what low levels of these gases, BrO in particular, had be detected by MAX-DOAS in these remote regions.

Gomez et al. (2014) retrieved the gas concentrations at a very long horizontal path of over 60 km from high mountain MAX-DOAS measurements at the Izaña Atmospheric observatory (28°18ˈN, 16°29″W, 2373 m a.s.l.) on the Canary Islands using the modified geometrical approach (MGA). The NO_2 mixing ratios were within the range of 20–40 ppt in the summer of 2011 (Gomez et al., 2014). Gil-Ojeda et al. (2015) applied the same technique to a longer data set obtained at the same station, and showed that the free tropospheric NO_2 mixing ratios varied in the range of 20–45 ppt between 2011 and 2013, with the lowest values in winter and highest values in summer. MAX-DOAS measurements were also performed at Zugspitze, Germany (47.5°N, 11°E, 2650 m a.s.l.) during February–July 2003 and Pico Espejo, Venezuela (8.5°N, 71°W, 4765 m a.s.l.) from March 2004 to February 2009. Based on the MGA method, the monthly mean mixing ratios of free tropospheric NO_2 were estimated to be in the range 60–100 ppt at Zugspitze and 8.5–15.5 ppt at Pico Espejo. The values for HCHO were in the range 500–950 ppt at Zugspitze and 255–385 ppt at Pico Espejo, respectively (Schreier et al., 2016).

BrO was detected directly in the mid-latitude marine environment for the first time, in the region north of the Canary Islands (around 35 °N, 13 °W),when a research cruise including ship MAX-DOAS (SMAX-DOAS) measurements was carried out over the Atlantic Ocean in October 2000 (Leser et al., 2003). Typical levels of BrO in the marine lower troposphere were <1 to 3.6 ppt in most cases, and upper limits of NO_2 for clean air in the Atlantic west of Africa was observed to be 24 to 100 ppt (Leser et al., 2003). BrO was measured by long-path MAX-DOAS (LP-MAX-DOAS) at the Mace Head observatory on the west coast of Ireland (53°20ˈ N,9°54ˈW) in August 2002. The BrO mixing ratios were shown to vary from below the detection limit (0.8 ppt) at night, to a maximum daytime concentration of 6.5 ppt, indicating that significant bromine activation occurs over the open ocean (Saiz-Lopez et al., 2004). Tropospheric BrO profiles over the remote Atlantic were obtained by aircraft/ship-based MAX-DOAS measurements by Volkamer et al. (2015). In the marine boundary layer (MBL) mixing ratios close to zero were obtained, which increase with altitude in the free troposphere. In the middle troposphere mixing ratios up to 1 ppt were found. Fitzenberger et al. (2000) derived BrO profiles from balloon borne measurements in Kiruna (Sweden) with mixing ratios up to about 1 ppt in the free troposphere.

It can be seen that the levels of NO_2 at WLG derived from this study are comparable to those measured by MAX-DOAS in other remote areas. However, the upper limit for the free tropospheric mixing ratios of BrO at WLG (about 0.3 ppt) derived from this study is lower than those observed under the MBL conditions at the same latitude band.

7 Conclusions

We made long-term ground-based MAX-DOAS measurements at the WLG WMO/GAW global baseline station during the period 2012–2015. For this study we analyzed the measured spectra to estimate the tropospheric background mixing ratios of different trace gases, including NO_2, SO_2, HCHO and BrO, from MAX-DOAS measurements at WLG.

For the spectral retrieval, we find that averaging of spectra increases the signal to noise ratio and thus reduces the statistical error of the spectral retrieval on one hand, and systematic errors caused by imperfect correction of the Ring effect tend to increase if an increasing number of spectra is averaged on other hand. Averages of 10 original spectra have been approved to be an ‘optimum option’ in the spectral analysis for this study. We determined the settings and spectral ranges for the retrieval of the different trace gases by a large number of dedicated sensitivity studies. We performed radiative transfer simulations with the RTM TRACY-2, which allows to explicitly consider the variation of the topography around the measurement station in viewing direction. From the simulations results, approximate relationships between the trace gas dSCDs (at 1 °elevation angle and low aerosol load: AOD = 0.1) and the corresponding volume mixing ratios are derived. We used the temporal variation and the spread of the colour index (CI) derived from our MAX-DOAS measurements to select measurement data for clear sky and low aerosol load, and then retrieved the corresponding daily averages and seasonal cycles of the trace gas dSCDs at elevation angles of 1 °, 6 °, 16 °.

For NO_2 and HCHO higher dSCDs are found for lower elevation angles than for higher elevation angles, indicating enhanced trace gas mixing ratios in the lower troposphere over WLG. For BrO the opposite dependence is found, reflecting the influence of stratospheric BrO. For SO_2 no clear elevation dependence is found. The highest NO_2 dSCDs are found in a period from April to June, most likely due to the long range transport of NO_2 and its reservoirs to WLG. From the dSCDs at 1 ° elevation, mixing ratios of NO_2 in the lower troposphere over WLG are estimated to be between about 5 ppt (January) and 70 ppt (May), and mixing ratios of SO_2 fall below 0.5 ppb. Mixing ratios of HCHO range between about 0.3 (winter) and 0.7 ppb (summer). These mixing ratios are most representative for atmospheric layers between about 4 and 5 km. Mixing ratios of BrO are estimated to be smaller than 0.3 ppt. Retrieving BrO in the continental background troposphere remains a challenge, which should be further addressed in future studies.

Data availability

The spectral analysis and RTM simulation results here are available upon request.

Author contributions

JM and TW designed the study. JM, JJ, JG, ZZ, JW, PL and GZ contributed to the measurements. TW, JM, SDörner, SDonner, JJ, SC, JP and JL contributed to the data analyses. TW and JM prepared the manuscript with consented by all co-authors.

Competing interests

The authors declare that they have no conflict of interest.

Special issue statement

This article is part of the special issue “Study of ozone, aerosols and radiation over the Tibetan Plateau (SOAR-TP) (ACP/AMT inter-journal SI)”. It is not associated with a conference.

Acknowledgements.

This work was funded by MOST (grant no. 2018YFC1505703) and NSFC (grant nos. 41275140 and 41875146). We thank all the staff from WLG for assisting measurement work.

References

Bauwens, M., Stavrakou, T., Müller, J. F., De Smedt, I., Van Roozendael, M., van der Werf, G. R., Wiedinmyer, C., Kaiser, J. W., Sindelarova, K., and Guenther, A.: Nine years of global hydrocarbon emissions based on source inversion of OMI formaldehyde observations, Atmos. Chem. Phys., 16, 10133-10158, 10.5194/acp-16-10133-2016, 2016.

Bobrowski, N., Honninger, G., Galle, B., and Platt, U.: Detection of bromine monoxide in a volcanic plume, Nature, 423, 273-276, 2003.

Coburn, S., Dix, B., Sinreich, R., and Volkamer, R.: The CU ground MAX-DOAS instrument: characterization of RMS noise limitations and first measurements near Pensacola, FL of BrO, IO, and CHOCHO, Atmos. Meas. Tech., 4, 2421-2439, 10.5194/amt-4-2421-2011, 2011.

De Mazière, M., Thompson, A. M., Kurylo, M. J., Wild, J. D., Bernhard, G., Blumenstock, T., Braathen, G. O., Hannigan, J. W., Lambert, J. C., Leblanc, T., McGee, T. J., Nedoluha, G., Petropavlovskikh, I., Seckmeyer, G., Simon, P. C., Steinbrecht, W., and Strahan, S. E.: The Network for the Detection of Atmospheric Composition Change (NDACC): history, status and perspectives, Atmos. Chem. Phys., 18, 4935-4964, 10.5194/acp-18-4935-2018, 2018.

De Smedt, I., Stavrakou, T., Hendrick, F., Danckaert, T., Vlemmix, T., Pinardi, G., Theys, N., Lerot, C., Gielen, C., Vigouroux, C., Hermans, C., Fayt, C., Veefkind, P., Müller, J. F., and Van Roozendael, M.: Diurnal, seasonal and long-term variations of global formaldehyde columns inferred from combined OMI and GOME-2 observations, Atmos. Chem. Phys., 15, 12519-12545, 10.5194/acp-15-12519-2015, 2015.

Dentener, F., Kinne, S., Bond, T., Boucher, O., Cofala, J., Generoso, S., Ginoux, P., Gong, S., Hoelzemann, J. J., Ito, A., Marelli, L., Penner, J. E., Putaud, J. P., Textor, C., Schulz, M., van der Werf, G. R., and Wilson, J.: Emissions of primary aerosol and precursor gases in the years 2000 and 1750 prescribed data-sets for AeroCom, Atmos. Chem. Phys., 6, 4321-4344, 10.5194/acp-6-4321-2006, 2006.

Fioletov, V. E., McLinden, C. A., Krotkov, N., Li, C., Joiner, J., Theys, N., Carn, S., and Moran, M. D.: A global catalogue of large SO2 sources and emissions derived from the Ozone Monitoring Instrument, Atmos. Chem. Phys., 16, 11497-11519, 10.5194/acp-16-11497-2016, 2016.

Fitzenberger, R., Bösch, H., Camy, Peyret, C., Chipperfield, M. P., Harder, H., Platt, U., Sinnhuber, B., M, Wagner, T., and Pfeilsticker, K.: First profile measurements of tropospheric BrO, Geophys. Res. Lett., 27, 2921-2924, 10.1029/2000gl011531, 2000.

Forster, P., Ramasway, V., Artaxo, P., Berntsen, T., Betts, R., Fahey, D. W., Haywood, J., Lean, J., Lowe, D. C., Myhre, G., Nganga, J., Prinn, R., Raga, G., Schulz, M., and Van Dorlando, R.: Changes in atmospheric constituents and in radiative forcing, in: Climate Change 2007: The Physical Science Basis. Contribution of Working Group I to the Fourth Assessment Report of the Intergovernmental Panel on Climate Change, edited by: Solomon, S., Qin, D., Manning, M., Chen, Z., Marquist, M., Averyt, K. B., Tignor, M., and Miller, H. L., Cambridge Univ. Press, Cambridge, U. K. and New York, U.S.A., 129-234, 2007.

Frieß, U., Hollwedel, J., König-Langlo, G., Wagner, T., and Platt, U.: Dynamics and chemistry of tropospheric bromine explosion events in the Antarctic coastal region, J. Geophys. Res., 109, D06305, 10.1029/2003jd004133, 2004.

Georgoulias, A. K., van der A, R. J., Stammes, P., Boersma, K. F., and Eskes, H. J.: Trends and trend reversal detection in two decades of tropospheric NO2 satellite observations, Atmos. Chem. Phys. Discuss., 2018, 1-38, 10.5194/acp-2018-988, 2018.

Gielen, C., Van Roozendael, M., Hendrick, F., Pinardi, G., Vlemmix, T., De Bock, V., De Backer, H., Fayt, C., Hermans, C., Gillotay, D., and Wang, P.: A simple and versatile cloud-screening method for MAX-DOAS retrievals, Atmos. Meas. Tech., 7, 3509-3527, 10.5194/amt-7-3509-2014, 2014.

Gil-Ojeda, M., Navarro-Comas, M., Gómez-Martín, L., Adame, J. A., Saiz-Lopez, A., Cuevas, C. A., González, Y., Puentedura, O., Cuevas, E., Lamarque, J. F., Kinninson, D., and Tilmes, S.: NO_2 seasonal evolution in the north subtropical free troposphere, Atmos. Chem. Phys., 15, 10567-10579, 10.5194/acp-15-10567-2015, 2015.

Gomez, L., Navarro-Comas, M., Puentedura, O., Gonzalez, Y., Cuevas, E., and Gil-Ojeda, M.: Long-path averaged mixing ratios of O_3 and NO2 in the free troposphere from mountain MAX-DOAS, Atmos. Meas. Tech., 7, 3373-3386, 10.5194/amt-7-3373-2014, 2014.

Granier, C., Bessagnet, B., Bond, T., D'Angiola, A., Denier van der Gon, H., Frost, G. J., Heil, A., Kaiser, J. W., Kinne, S., Klimont, Z., Kloster, S., Lamarque, J.-F., Liousse, C., Masui, T., Meleux, F., Mieville, A., Ohara, T., Raut, J.-C., Riahi, K., Schultz, M. G., Smith, S. J., Thompson, A., van Aardenne, J., van der Werf, G. R., and van Vuuren, D. P.: Evolution of anthropogenic and biomass burning emissions of air pollutants at global and regional scales during the 1980–2010 period, Climatic Change, 109, 163, 10.1007/s10584-011-0154-1, 2011.

Hönninger, G., and Platt, U.: Observations of BrO and its vertical distribution during surface ozone depletion at Alert, Atmospheric Environment, 36, 2481-2489, 2002.

Hönninger, G., von Friedeburg, C., and Platt, U.: Multi axis differential optical absorption spectroscopy (MAX-DOAS), Atmos. Chem. Phys., 4, 231-254, 10.5194/acp-4-231-2004, 2004.

Hammer, M. S., Martin, R. V., Li, C., Torres, O., Manning, M., and Boys, B. L.: Insight into global trends in aerosol composition from 2005 to 2015 inferred from the OMI Ultraviolet Aerosol Index, Atmos. Chem. Phys., 18, 8097-8112, 10.5194/acp-18-8097-2018, 2018.

Harder, H., Camy, Peyret, C., Ferlemann, F., Fitzenberger, R., Hawat, T., Osterkamp, H., Schneider, M., Perner, D., Platt, U., Vradelis, P., and Pfeilsticker, K.: Stratospheric BrO profiles measured at different latitudes and seasons: Atmospheric observations, Geophys. Res. Lett., 25, 3843-3846, 10.1029/1998gl900026, 1998.

Hendrick, F., Van Roozendael, M., Chipperfield, M. P., Dorf, M., Goutail, F., Yang, X., Fayt, C., Hermans, C., Pfeilsticker, K., Pommereau, J. P., Pyle, J. A., Theys, N., and De Mazière, M.: Retrieval of stratospheric and tropospheric BrO profiles and columns using ground-based zenith-sky DOAS observations at Harestua, 60° N, Atmos. Chem. Phys., 7, 4869-4885, 10.5194/acp-7-4869-2007, 2007.

Hendrick, F., Müller, J. F., Clémer, K., Wang, P., De Mazière, M., Fayt, C., Gielen, C., Hermans, C., Ma, J. Z., Pinardi, G., Stavrakou, T., Vlemmix, T., and Van Roozendael, M.: Four years of ground-based MAX-DOAS observations of HONO and NO_2 in the Beijing area, Atmos. Chem. Phys., 14, 765-781, 10.5194/acp-14-765-2014, 2014.

Jin, J., Ma, J., Lin, W., Zhao, H., Shaiganfar, R., Beirle, S., and Wagner, T.: MAX-DOAS measurements and satellite validation of tropospheric NO_2 and SO_2 vertical column densities at a rural site of North China, Atmospheric Environment, 133, 12-25, http://dx.doi.org/10.1016/j.atmosenv.2016.03.031, 2016.

Klimont, Z., Kupiainen, K., Heyes, C., Purohit, P., Cofala, J., Rafaj, P., Borken-Kleefeld, J., and Schöpp, W.: Global anthropogenic emissions of particulate matter including black carbon, Atmos. Chem. Phys., 17, 8681-8723, 10.5194/acp-17-8681-2017, 2017.

Krotkov, N. A., McLinden, C. A., Li, C., Lamsal, L. N., Celarier, E. A., Marchenko, S. V., Swartz, W. H., Bucsela, E. J., Joiner, J., Duncan, B. N., Boersma, K. F., Veefkind, J. P., Levelt, P. F., Fioletov, V. E., Dickerson, R. R., He, H., Lu, Z., and Streets, D. G.: Aura OMI observations of regional SO2 and NO2 pollution changes from 2005 to 2015, Atmos. Chem. Phys., 16, 4605-4629, 10.5194/acp-16-4605-2016, 2016.

Lübcke, P., Lampel, J., Arellano, S., Bobrowski, N., Dinger, F., Galle, B., Garzón, G., Hidalgo, S., Chacón Ortiz, Z., Vogel, L., Warnach, S., and Platt, U.: Retrieval of absolute SO2 column amounts from scattered-light spectra: implications for the evaluation of data from automated DOAS networks, Atmos. Meas. Tech., 9, 5677-5698, 10.5194/amt-9-5677-2016, 2016.

Lampel, J., Zielcke, J., Schmitt, S., Pöhler, D., Frieß, U., Platt, U., and Wagner, T.: Detection of O4 absorption around 328 and 419 nm in measured atmospheric absorption spectra, Atmos. Chem. Phys., 18, 1671-1683, 10.5194/acp-18-1671-2018, 2018.

Lary, D. J.: Halogens and the chemistry of the free troposphere, Atmos. Chem. Phys., 5, 227-237, 10.5194/acp-5-227-2005, 2005.

Lee, D. S., Köhler, I., Grobler, E., Rohrer, F., Sausen, R., Gallardo-Klenner, L., Olivier, J. G. J., Dentener, F. J., and Bouwman, A. F.: Estimations of global no, emissions and their uncertainties, Atmospheric Environment, 31, 1735-1749, https://doi.org/10.1016/S1352-2310(96)00327-5, 1997.

Lelieveld, J., Gromov, S., Pozzer, A., and Taraborrelli, D.: Global tropospheric hydroxyl distribution, budget and reactivity, Atmospheric Chemistry and Physics, 16, 12477-12493, 10.5194/acp-16-12477-2016, 2016.

Leser, H., Hönninger, G., and Platt, U.: MAX-DOAS measurements of BrO and NO2 in the marine boundary layer, Geophys. Res. Lett., 30, 1537, 10.1029/2002gl015811, 2003.

Li, C., Martin, R. V., van Donkelaar, A., Boys, B. L., Hammer, M. S., Xu, J.-W., Marais, E. A., Reff, A., Strum, M., Ridley, D. A., Crippa, M., Brauer, M., and Zhang, Q.: Trends in Chemical Composition of Global and Regional Population-

Weighted Fine Particulate Matter Estimated for 25 Years, Environmental Science & Technology, 51, 11185-11195, 10.1021/acs.est.7b02530, 2017.

Lin, W., Xu, X., Yu, X., Zhang, X., and Huang, J.: Observed levels and trends of gaseous SO_2 and HNO_3 at Mt. Waliguan, China: Results from 1997 to 2009, Journal of Environmental Sciences, 25, 726-734, https://doi.org/10.1016/S1001-0742(12)60143-0, 2013.

Luo, Y., Si, F., Zhou, H., Dou, K., Liu, Y., and Liu, W.: Observations and source investigations of the boundary layer bromine monoxide (BrO) in the Ny-Ålesund Arctic, Atmos. Chem. Phys., 18, 9789-9801, 10.5194/acp-18-9789-2018, 2018.

Ma, J., Tang, J., Zhou, X., and Zhang, X.: Estimates of the chemical budget for ozone at Waliguan Observatory J. Atmos. Chem., 41, 21-48, 10.1023/A:1013892308983 2002a.

Ma, J., Zhou, X., and Hauglustaine, D.: Summertime tropospheric ozone over China simulated with a regional chemical transport model 2. Source contributions and budget, Journal of Geophysical Research: Atmospheres, 107, 4612, 10.1029/2001jd001355, 2002b.

Ma, J. Z., Chen, Y., Wang, W., Yan, P., Liu, H. J., Yang, S. Y., Hu, Z. J., and Lelieveld, J.: Strong air pollution causes widespread haze-clouds over China, J. Geophys. Res., 115, D18204, 10.1029/2009jd013065, 2010.

Ma, J. Z., Wang, W., Chen, Y., Liu, H. J., Yan, P., Ding, G. A., Wang, M. L., Sun, J., and Lelieveld, J.: The IPAC-NC field campaign: a pollution and oxidization pool in the lower atmosphere over Huabei, China, Atmos. Chem. Phys., 12, 3883-3908, 10.5194/acp-12-3883-2012, 2012.

Ma, J. Z., Beirle, S., Jin, J. L., Shaiganfar, R., Yan, P., and Wagner, T.: Tropospheric NO_2 vertical column densities over Beijing: results of the first three years of ground-based MAX-DOAS measurements (2008-2011) and satellite validation, Atmos. Chem. Phys., 13, 1547-1567, 10.5194/acp-13-1547-2013, 2013.

Martin, M., Pöhler, D., Seitz, K., Sinreich, R., and Platt, U.: BrO measurements over the Eastern North-Atlantic, Atmos. Chem. Phys., 9, 9545-9554, 2009.

Meng, Z.-Y., Xu, X.-B., Wang, T., Zhang, X.-Y., Yu, X.-L., Wang, S.-F., Lin, W.-L., Chen, Y.-Z., Jiang, Y.-A., and An, X.-Q.: Ambient sulfur dioxide, nitrogen dioxide, and ammonia at ten background and rural sites in China during 2007–2008, Atmospheric Environment, 44, 2625-2631, https://doi.org/10.1016/j.atmosenv.2010.04.008, 2010.

Mu, Y., Pang, X., Quan, J., and Zhang, X.: Atmospheric carbonyl compounds in Chinese background area: A remote mountain of the Qinghai-Tibetan Plateau, Journal of Geophysical Research: Atmospheres, 112, D22302, 10.1029/2006jd008211, 2007.

Peterson, P. K., Simpson, W. R., Pratt, K. A., Shepson, P. B., Frieß, U., Zielcke, J., Platt, U., Walsh, S. J., and Nghiem, S. V.: Dependence of the vertical distribution of bromine monoxide in the lower troposphere on meteorological factors such as wind speed and stability, Atmos. Chem. Phys., 15, 2119-2137, 10.5194/acp-15-2119-2015, 2015.

Peterson, P. K., Pöhler, D., Sihler, H., Zielcke, J., General, S., Frieß, U., Platt, U., Simpson, W. R., Nghiem, S. V., Shepson, P. B., Stirm, B. H., Dhaniyala, S., Wagner, T., Caulton, D. R., Fuentes, J. D., and Pratt, K. A.: Observations of bromine monoxide transport in the Arctic sustained on aerosol particles, Atmos. Chem. Phys., 17, 7567-7579, 10.5194/acp-17-7567-2017, 2017.

Platt, U., and Hönninger, G.: The role of halogen species in the troposphere, Chemosphere, 52, 325-338, 2003.

Prados-Roman, C., Gómez-Martín, L., Puentedura, O., Navarro-Comas, M., Iglesias, J., de Mingo, J. R., Pérez, M., Ochoa, H., Barlasina, M. E., Carbajal, G., and Yela, M.: Reactive bromine in the low troposphere of Antarctica: estimations at two research sites, Atmos. Chem. Phys., 18, 8549-8570, 10.5194/acp-18-8549-2018, 2018.

Richter, A., Wittrock, F., Ladstätter-Weissenmayer, A., and Burrows, J. P.: GOME measurements of stratospheric and tropospheric BrO, Adv. Space Res., 29, 1667–1672, 2002.

Roscoe, H. K., Brough, N., Jones, A. E., Wittrock, F., Richter, A., Van Roozendael, M., and Hendrick, F.: Resolution of an important discrepancy between remote and in-situ measurements of tropospheric BrO during Antarctic enhancements, Atmos. Meas. Tech. Discuss., 2012, 5419-5448, 10.5194/amtd-5-5419-2012, 2012.

Saiz-Lopez, A., Plane, J. M. C., and Shillito, J. A.: Bromine oxide in the mid-latitude marine boundary layer, Geophys. Res. Lett., 31, L03111, 10.1029/2003gl018956, 2004.

Schreier, S. F., Richter, A., Wittrock, F., and Burrows, J. P.: Estimates of free-tropospheric NO2 and HCHO mixing ratios derived from high-altitude mountain MAX-DOAS observations at midlatitudes and in the tropics, Atmos. Chem. Phys., 16, 2803-2817, 10.5194/acp-16-2803-2016, 2016.

Seinfeld, J. H., and Pandis, S. N.: Atmospheric Chemistry and Physics: From Air Pollution to Climate Change (Second Edition), Hohn Wiley & Sons. Inc., Hoboken, New Jersey, 2006.

Simpson, W. R., Peterson, P. K., Frieß, U., Sihler, H., Lampel, J., Platt, U., Moore, C., Pratt, K., Shepson, P., Halfacre, J., and Nghiem, S. V.: Horizontal and vertical structure of reactive bromine events probed by bromine monoxide MAX-DOAS, Atmos. Chem. Phys., 17, 9291-9309, 10.5194/acp-17-9291-2017, 2017.

Stavrakou, T., Müller, J. F., De Smedt, I., Van Roozendael, M., van der Werf, G. R., Giglio, L., and Guenther, A.: Evaluating the performance of pyrogenic and biogenic emission inventories against one decade of space-based formaldehyde columns, Atmos. Chem. Phys., 9, 1037-1060, 10.5194/acp-9-1037-2009, 2009.

Stohl, A., Aamaas, B., Amann, M., Baker, L. H., Bellouin, N., Berntsen, T. K., Boucher, O., Cherian, R., Collins, W., Daskalakis, N., Dusinska, M., Eckhardt, S., Fuglestvedt, J. S., Harju, M., Heyes, C., Hodnebrog, Ø., Hao, J., Im, U., Kanakidou, M., Klimont, Z., Kupiainen, K., Law, K. S., Lund, M. T., Maas, R., MacIntosh, C. R., Myhre, G., Myriokefalitakis, S., Olivié, D., Quaas, J., Quennehen, B., Raut, J. C., Rumbold, S. T., Samset, B. H., Schulz, M., Seland, Ø., Shine, K. P., Skeie, R. B., Wang, S., Yttri, K. E., and Zhu, T.: Evaluating the climate and air quality impacts of short-lived pollutants, Atmos. Chem. Phys., 15, 10529-10566, 10.5194/acp-15-10529-2015, 2015.

Stutz, J., Ackermann, R., Fast, J. D., and Barrie, L.: Atmospheric reactive chlorine and bromine at the Great Salt Lake, Utah, Geophys. Res. Lett., 29, 1380, 10.1029/2002gl014812, 2002.

Tang, J., Wen, Y. P., Xu, X. B., Zheng, X. D., Guo, S., and Zhao, Y. C.: China Global Atmosphere Watch Baseline Observatory and its measurement program: In: CAMS Annual Report 1994-1995, Beijing, 56-65, 1995.

Theys, N., Van Roozendael, M., Hendrick, F., Fayt, C., Hermans, C., Baray, J. L., Goutail, F., Pommereau, J. P., and De Mazière, M.: Retrieval of stratospheric and tropospheric BrO columns from multi-axis DOAS measurements at Reunion Island (21°S, 56°E), Atmos. Chem. Phys., 7, 4733-4749, 10.5194/acp-7-4733-2007, 2007.

Tulet, P., Di Muro, A., Colomb, A., Denjean, C., Duflot, V., Arellano, S., Foucart, B., Brioude, J., Sellegri, K., Peltier, A., Aiuppa, A., Barthe, C., Bhugwant, C., Bielli, S., Boissier, P., Boudoire, G., Bourrianne, T., Brunet, C., Burnet, F., Cammas, J. P., Gabarrot, F., Galle, B., Giudice, G., Guadagno, C., Jeamblu, F., Kowalski, P., Leclair de Bellevue, J., Marquestaut, N., Mékies, D., Metzger, J. M., Pianezze, J., Portafaix, T., Sciare, J., Tournigand, A., and Villeneuve, N.: First results of the Piton de la Fournaise STRAP 2015 experiment: multidisciplinary tracking of a volcanic gas and aerosol plume, Atmos. Chem. Phys., 17, 5355-5378, 10.5194/acp-17-5355-2017, 2017.

Van Roozendael, M., Wagner, T., Richter, A., Pundt, I., Arlander, D., Burrows, J. P., Chipperfield, M., Fayt, C., Johnston, P. V., Lambert, J.-C., Kreher, K., Pfeilsticker, K., Platt, U., Pommereau, J.-P., Sinnhuber, B.-M., Tornkvist, K. K., and

Wittrock, F.: Intercomparison of BrO measurements from ERS-2 GOME, ground-based and balloon platforms, Adv. Space Res., 29, 1661–1666, 2002.

Van Roozendael, M., Fayt, C., Post, P., Hermans, C., and Lambert, J.-C.: Retrieval of BrO and NO_2 from UV-Visible Observations, in: Sounding the troposphere from space: a new Era for Atmospheric Chemistry, The TROPOSAT Final Report, edited by: Borrell, P., Borrell, P. M., Burrows, J. P., and Platt, U., Springer, Dordrecht, 155–166, 2003.

Volkamer, R., Baidar, S., Campos, T. L., Coburn, S., DiGangi, J. P., Dix, B., Eloranta, E. W., Koenig, T. K., Morley, B., Ortega, I., Pierce, B. R., Reeves, M., Sinreich, R., Wang, S., Zondlo, M. A., and Romashkin, P. A.: Aircraft measurements of BrO, IO, glyoxal, NO_2, H_2O, O_2–O_2 and aerosol extinction profiles in the tropics: comparison with aircraft-/ship-based in situ and lidar measurements, Atmos. Meas. Tech., 8, 2121-2148, 10.5194/amt-8-2121-2015, 2015.

von Glasow, R., von Kuhlmann, R., Lawrence, M. G., Platt, U., and Crutzen, P. J.: Impact of reactive bromine chemistry in the troposphere, Atmos. Chem. Phys., 4, 2481-2497, 10.5194/acp-4-2481-2004, 2004.

von Glasow, R., and Crutzen, P. J.: Tropospheric Halogen Chemistry, in: Treatise on Geochemistry Update1, edited by: Holland, H. D., and Turekian, K. K., Elsevier-Pergamon, Oxford, UK, 1–67, 2007.

Wagner, T., Dix, B., Friedeburg, C. v., Frieß, U., Sanghavi, S., Sinreich, R., and Platt, U.: MAX-DOAS O_4 measurements: A new technique to derive information on atmospheric aerosols -- Principles and information content, J. Geophys. Res., 109, D22205, 10.1029/2004jd004904, 2004.

Wagner, T., Burrows, J. P., Deutschmann, T., Dix, B., von Friedeburg, C., Frieß, U., Hendrick, F., Heue, K. P., Irie, H., Iwabuchi, H., Kanaya, Y., Keller, J., McLinden, C. A., Oetjen, H., Palazzi, E., Petritoli, A., Platt, U., Postylyakov, O., Pukite, J., Richter, A., van Roozendael, M., Rozanov, A., Rozanov, V., Sinreich, R., Sanghavi, S., and Wittrock, F.: Comparison of box-air-mass-factors and radiances for Multiple-Axis Differential Optical Absorption Spectroscopy (MAX-DOAS) geometries calculated from different UV/visible radiative transfer models, Atmos. Chem. Phys., 7, 1809-1833, 10.5194/acp-7-1809-2007, 2007a.

Wagner, T., Ibrahim, O., Sinreich, R., Frieß, U., von Glasow, R., and Platt, U.: Enhanced tropospheric BrO over Antarctic sea ice in mid winter observed by MAX-DOAS on board the research vessel Polarstern, Atmos. Chem. Phys., 7, 3129-3142, 10.5194/acp-7-3129-2007, 2007b.

Wagner, T., Apituley, A., Beirle, S., Dörner, S., Friess, U., Remmers, J., and Shaiganfar, R.: Cloud detection and classification based on MAX-DOAS observations, Atmos. Meas. Tech., 7, 1289-1320, 10.5194/amt-7-1289-2014, 2014.

Wagner, T., Beirle, S., Remmers, J., Shaiganfar, R., and Wang, Y.: Absolute calibration of the colour index and O4 absorption derived from Multi AXis (MAX-)DOAS measurements and their application to a standardised cloud classification algorithm, Atmos. Meas. Tech., 9, 4803-4823, 10.5194/amt-9-4803-2016, 2016.

Wang, T., Wong, H. L. A., Tang, J., Ding, A., Wu, W. S., and Zhang, X. C.: On the origin of surface ozone and reactive nitrogen observed at a remote mountain site in the northeastern Qinghai-Tibetan Plateau, western China, Journal of Geophysical Research: Atmospheres, 111, D08303, 10.1029/2005jd006527, 2006.

Wang, T., Hendrick, F., Wang, P., Tang, G., Clémer, K., Yu, H., Fayt, C., Hermans, C., Gielen, C., Müller, J. F., Pinardi, G., Theys, N., Brenot, H., and Van Roozendael, M.: Evaluation of tropospheric SO2 retrieved from MAX-DOAS measurements in Xianghe, China, Atmos. Chem. Phys., 14, 11149-11164, 10.5194/acp-14-11149-2014, 2014.

Wang, Y., Lampel, J., Xie, P., Beirle, S., Li, A., Wu, D., and Wagner, T.: Ground-based MAX-DOAS observations of tropospheric aerosols, NO2, SO2 and HCHO in Wuxi, China, from 2011 to 2014, Atmos. Chem. Phys., 17, 2189-2215, 10.5194/acp-17-2189-2017, 2017.

Werner, B., Stutz, J., Spolaor, M., Scalone, L., Raecke, R., Festa, J., Colosimo, S. F., Cheung, R., Tsai, C., Hossaini, R., Chipperfield, M. P., Taverna, G. S., Feng, W., Elkins, J. W., Fahey, D. W., Gao, R. S., Hintsa, E. J., Thornberry, T. D., Moore, F. L., Navarro, M. A., Atlas, E., Daube, B. C., Pittman, J., Wofsy, S., and Pfeilsticker, K.: Probing the subtropical lowermost stratosphere and the tropical upper troposphere and tropopause layer for inorganic bromine, Atmos. Chem. Phys., 17, 1161-1186, 10.5194/acp-17-1161-2017, 2017.

Wittrock, F., Oetjen, H., Richter, A., Fietkau, S., Medeke, T., Rozanov, A., and Burrows, J. P.: MAX-DOAS measurements of atmospheric trace gases in Ny-Ålesund - Radiative transfer studies and their application, Atmos. Chem. Phys., 4, 955-966, 10.5194/acp-4-955-2004, 2004.

Xing, J., Mathur, R., Pleim, J., Hogrefe, C., Gan, C. M., Wong, D. C., Wei, C., Gilliam, R., and Pouliot, G.: Observations and modeling of air quality trends over 1990–2010 across the Northern Hemisphere: China, the United States and Europe, Atmos. Chem. Phys., 15, 2723-2747, 10.5194/acp-15-2723-2015, 2015.

Xue, L. K., Wang, T., Zhang, J. M., Zhang, X. C., Deliger, Poon, C. N., Ding, A. J., Zhou, X. H., Wu, W. S., Tang, J., Zhang, Q. Z., and Wang, W. X.: Source of surface ozone and reactive nitrogen speciation at Mount Waliguan in western China: New insights from the 2006 summer study, Journal of Geophysical Research: Atmospheres, 116, D07306, 10.1029/2010jd014735, 2011.

Xue, L. K., Wang, T., Guo, H., Blake, D. R., Tang, J., Zhang, X. C., Saunders, S. M., and Wang, W. X.: Sources and photochemistry of volatile organic compounds in the remote atmosphere of western China: results from the Mt. Waliguan Observatory, Atmos. Chem. Phys., 13, 8551-8567, 10.5194/acp-13-8551-2013, 2013.

Yang, X., Cox, R. A., Warwick, N. J., Pyle, J. A., Carver, G. D., O'Connor, F. M., and Savage, N. H.: Tropospheric bromine chemistry and its impacts on ozone: A model study, J. Geophys. Res., 110, D23311, 10.1029/2005jd006244, 2005.

Yang, X., Pyle, J. A., Cox, R. A., Theys, N., and Van Roozendael, M.: Snow-sourced bromine and its implications for polar tropospheric ozone, Atmos. Chem. Phys., 10, 7763-7773, 10.5194/acp-10-7763-2010, 2010.

Yu, X., Tang, J., Li, X. S., and Liang, B. S.: Observation and analysis of SO_2 and NO_2 in clean air of western China, Quarterly J. Applied Meteorology, 8, 62-68, 1997.

Zhao, B., Wang, P., Ma, J. Z., Zhu, S., Pozzer, A., and Li, W.: A high-resolution emission inventory of primary pollutants for the Huabei region, China, Atmos. Chem. Phys., 12, 481-501, 10.5194/acp-12-481-2012, 2012.

Ziemke, J. R., Oman, L. D., Strode, S. A., Douglass, A. R., Olsen, M. A., McPeters, R. D., Bhartia, P. K., Froidevaux, L., Labow, G. J., Witte, J. C., Thompson, A. M., Haffner, D. P., Kramarova, N. A., Frith, S. M., Huang, L. K., Jaross, G. R., Seftor, C. J., Deland, M. T., and Taylor, S. L.: Trends in Global Tropospheric Ozone Inferred from a Composite Record of TOMS/OMI/MLS/OMPS Satellite Measurements and the MERRA-2 GMI Simulation, Atmos. Chem. Phys. Discuss., 2018, 1-29, 10.5194/acp-2018-716, 2018.

Table 1 Overview on the different fitting ranges and systematic and random errors for the retrieved trace gas dSCDs (for spectra averaged from 10 original spectra). More details are found in the Supplement.

	NO_2	SO_2	HCHO	BrO
Wavelength range (nm)	399 – 426	306 – 325	314 – 358	314 – 358
Systematic error (molec/cm^2)	6e14	8e15	4e15	3e12
Random error (molec/cm^2)	2e15	1.3e16	9e15	1.1e13

Table 2. Comparisons between trace gas mixing ratios at WLG and those recorded in other remote areas at low latitudes.

Location	Period	Method	NO_2 (ppt)	SO_2 (ppb)	HCHO (ppb)	BrO (ppt)	Reference
WLG	2012-2015	MAX-DOAS	5–70	<0.5	0.3–0.7	< 0.3	This study
WLG	winter	MAX-DOAS	5				This study
WLG	spring	MAX-DOAS	70				This study
WLG	Jan 1996	SP/ICG	22				Ma et al., 2002a
WLG	Jul 1996	SP/ICG	48				Ma et al., 2002a
WLG	2008	SP/SPM/ICG	600	0.7			Meng et al., 2010
WLG	1997-2009	SP/ICG		0.45			Lin et al, 2013
WLG	summer 2006	CLS/PhC	280				Xue et al., 2011
WLG	spring 2003	CLS/assuming	280				Xue et al., 2013
WLG	summer 2003	CLS/assuming	180				Xue et al., 2013
WLG	Aug-Sept 2005	SGC/HPLC			4.16		Mu et al., 2007
WLG	Dec 2005	SGC/HPLC			1.48		Mu et al., 2007
Izaña	summer 2011	MAX-DOAS	20–40				Gomez et al., 2014
Izaña	2011-2013	MAX-DOAS	20–45				Gil-Ojeda et al., 2015
Zugspitze	Feb-July 2003	MAX-DOAS	60–100		0.26–0.39		Schreier et al., 2016
Pico Espejo	2004- 2009	MAX-DOAS	9–16		0.50–0.95		Schreier et al., 2016
Atlantic MBL	Oct 2000	SMAX-DOAS	24–200			<1 –3.6	Leser et al., 2003
Kiruna (Sweden)	Aug 1998 & Feb 1999	Balloon DOAS				0.3 –1.2	Fitzenberger et al., 2000
Mace Head	Aug 2002	LP-DOAS				<0.8–6.5	Saiz-Lopez et al., 2004
Atlantic	Jan-Feb 2012	Ship/aircraft-based MAX-DOAS				0 –2	Volkamer et al., 2015

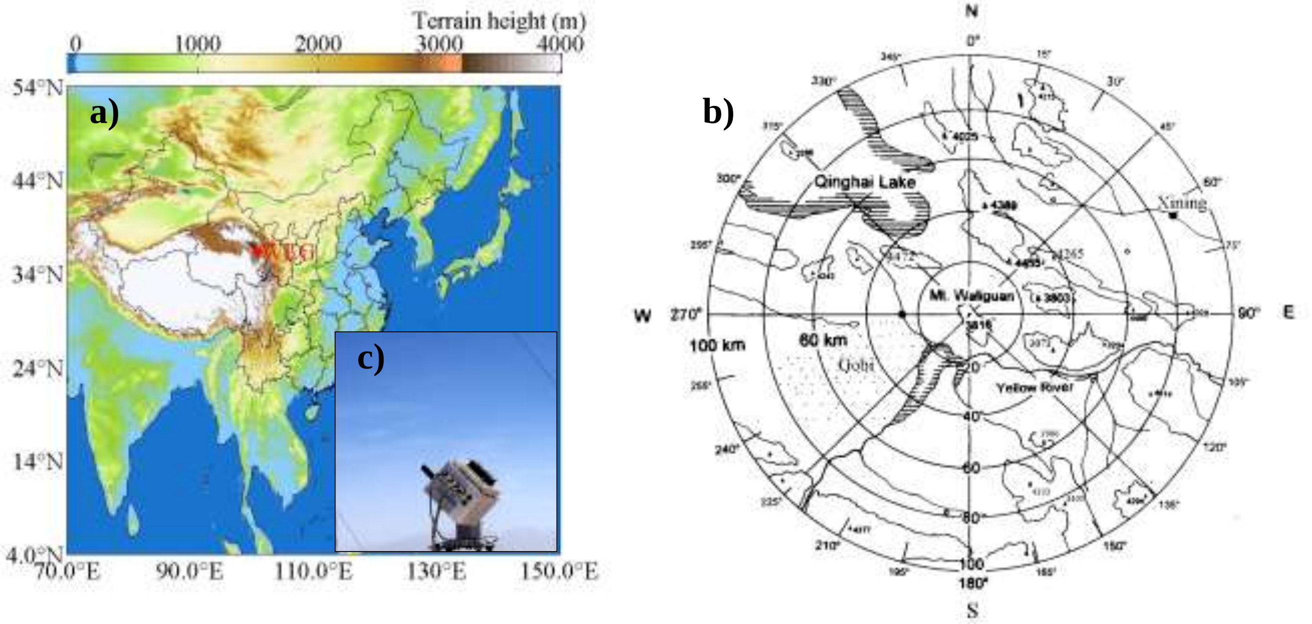

Figure 1 (a) Position of Mt Waliguan in East Asia. **(b)** Surrounding topography within 100 km distance from WLG. **(c)** The MAX-DOAS instrument installed at WLG.

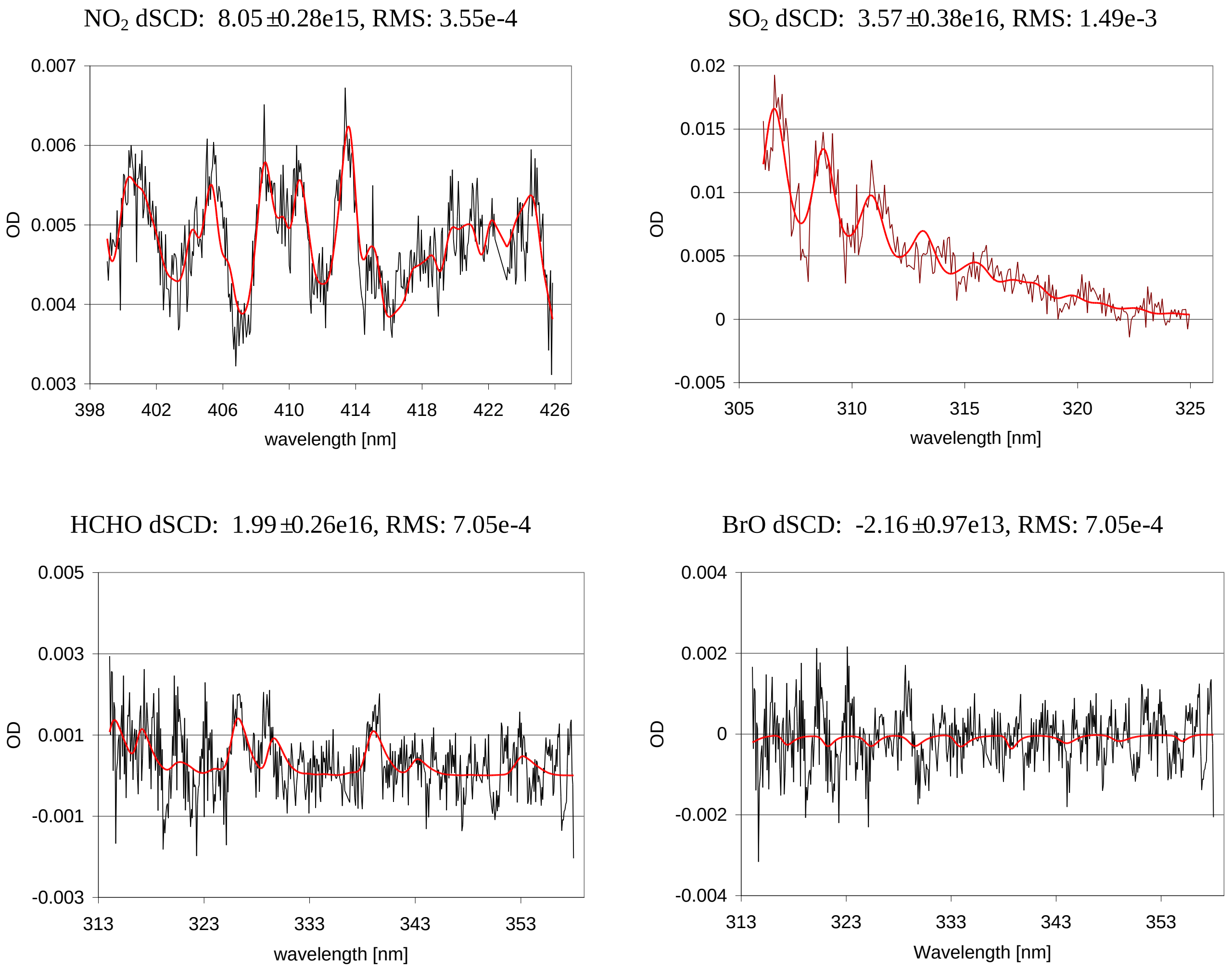

NO_2 dSCD: 8.05±0.28e15, RMS: 3.55e-4

SO_2 dSCD: 3.57±0.38e16, RMS: 1.49e-3

HCHO dSCD: 1.99±0.26e16, RMS: 7.05e-4

BrO dSCD: -2.16±0.97e13, RMS: 7.05e-4

Figure 2 Fit result for NO_2, SO_2, HCHO, and BrO for a spectrum (average of 10 original spectra) taken on 13 May 2013 (00:34 – 04:19) at 1 °elevation. On this day, enhanced absorptions of SO_2 and NO_2 were observed.

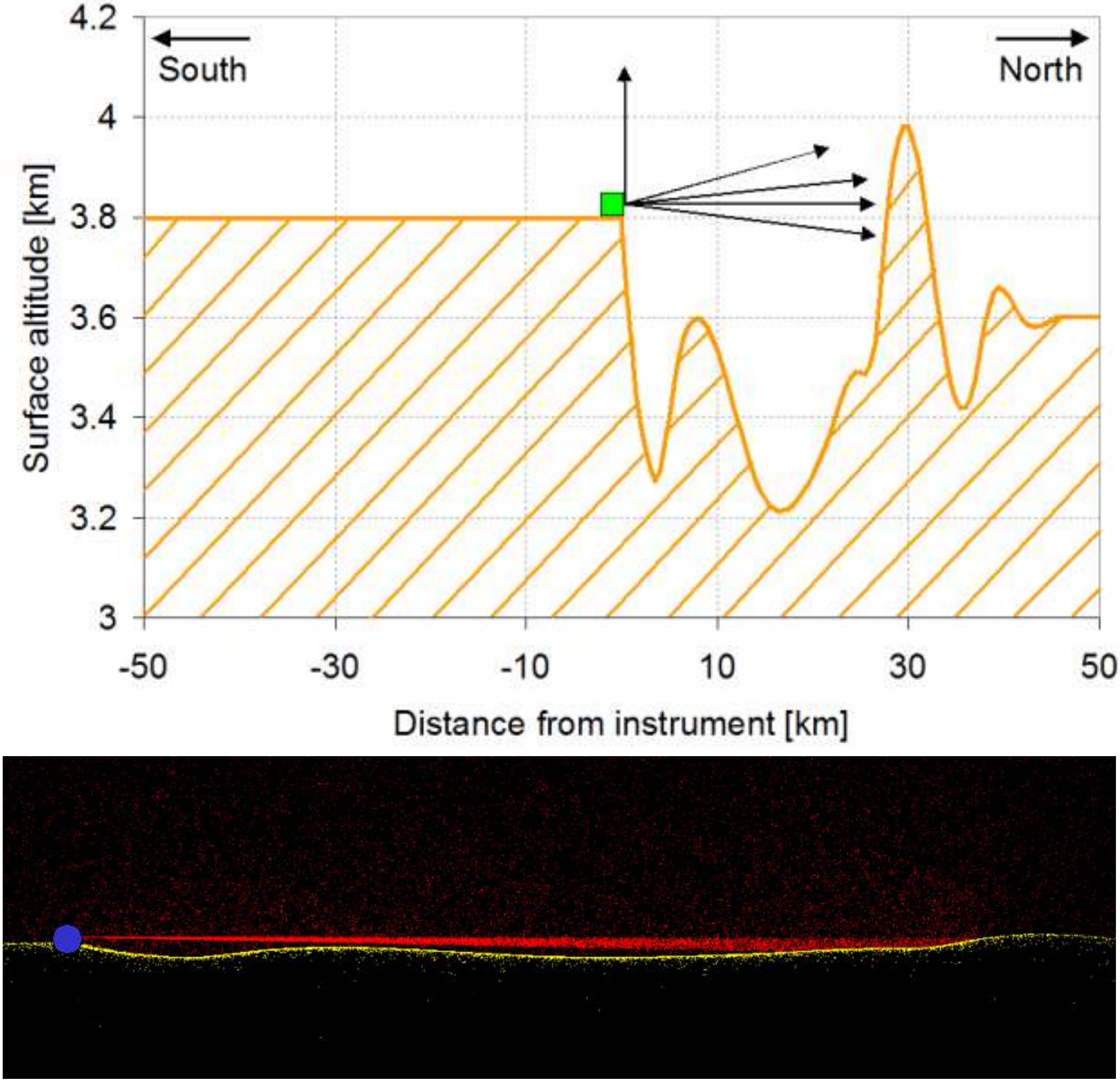

Figure 3 Top: Variation of the surface altitude in viewing direction (towards the North). The variation of the surface altitude across the viewing direction was not explicitly considered to minimise the computational effort. For the same reason, also the topography ‘behind’ the instrument, towards the South was assumed to be flat. **Bottom:** Illustration of the results of the radiative transfer simulations for the area between the instrument and the high mountain in 30 km distance. The blue dot indicates the position of the instrument. The small red and yellow dots indicate Rayleigh-scattering events and surface reflection of the simulated solar photons, respectively.

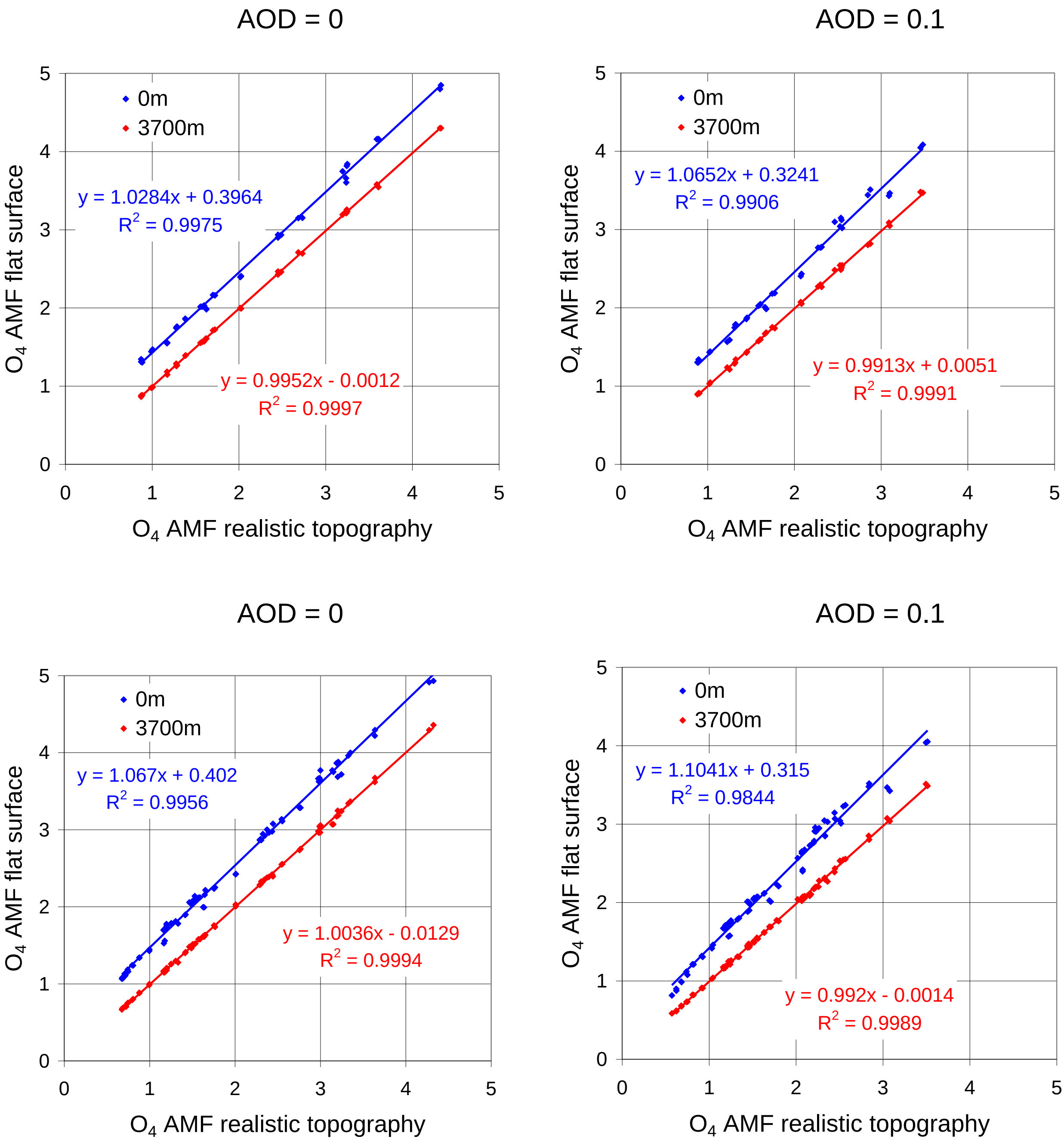

Figure 4 Comparison of simulated O_4 AMFs for different choices of the surface topography. Results for flat surfaces at sea level (blue) or 3700m (red) are plotted versus the results for a realistic surface topography (see Fig. 3). **Top:** results for winter; and **bottom:** results for summer. **Left:** results for simulation without aerosols; and **right:** results for an AOD of 0.1.

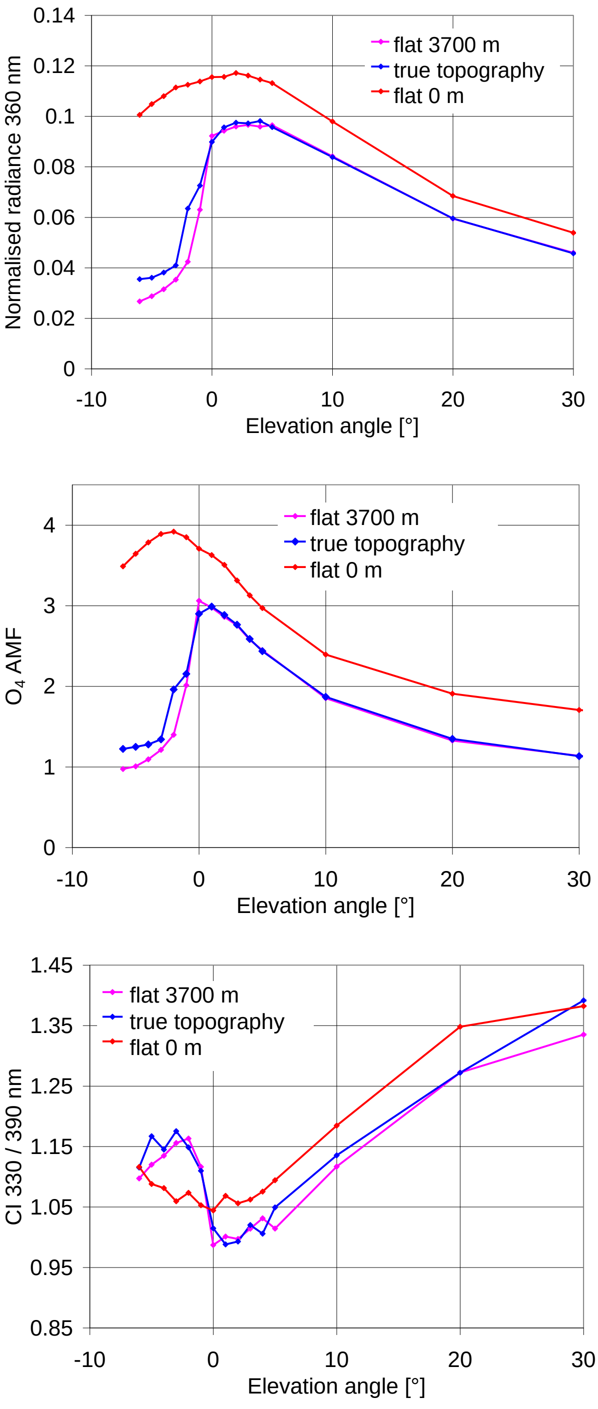

Figure 5 Simulation results of the radiance **(top)**, O_4 AMF **(middle)**, and colour index **(bottom)** for different choices of the surface topography as function of the elevation angle (including negative elevation angles). Simulation results are for summer noontime (see also Fig. S3 in the supplement).

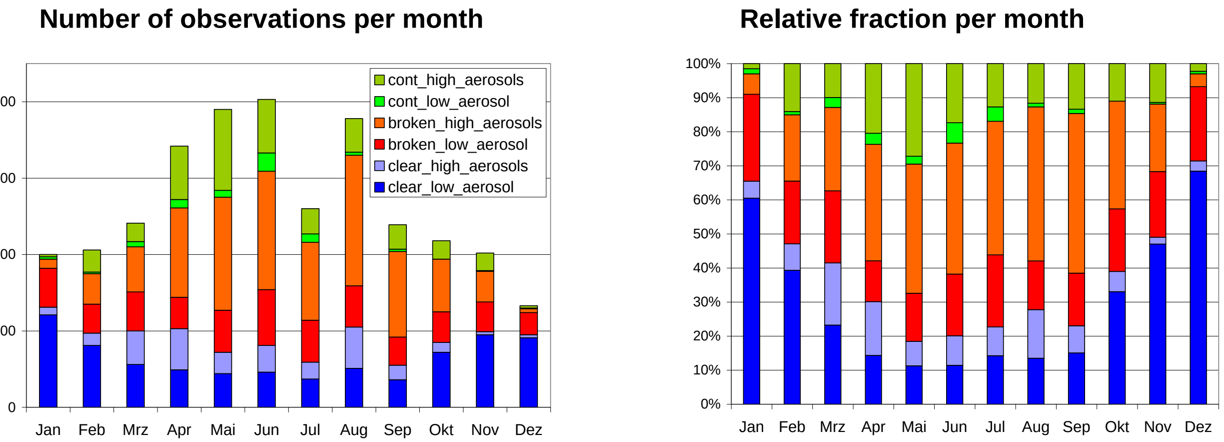

Figure 6 Absolute **(left)** and relative **(right)** frequency of the different sky conditions. The statistics is based on the number of observations at 1 °elevation angle of spectra averaged from 10 original spectra (April 2012 – April 2015). Only measurements with more than 800 scans are considered. The basic colours indicate the cloud properties (clear, broken clouds, continuous clouds). The full or light colours indicate observations with low or high aerosol loads, respectively.

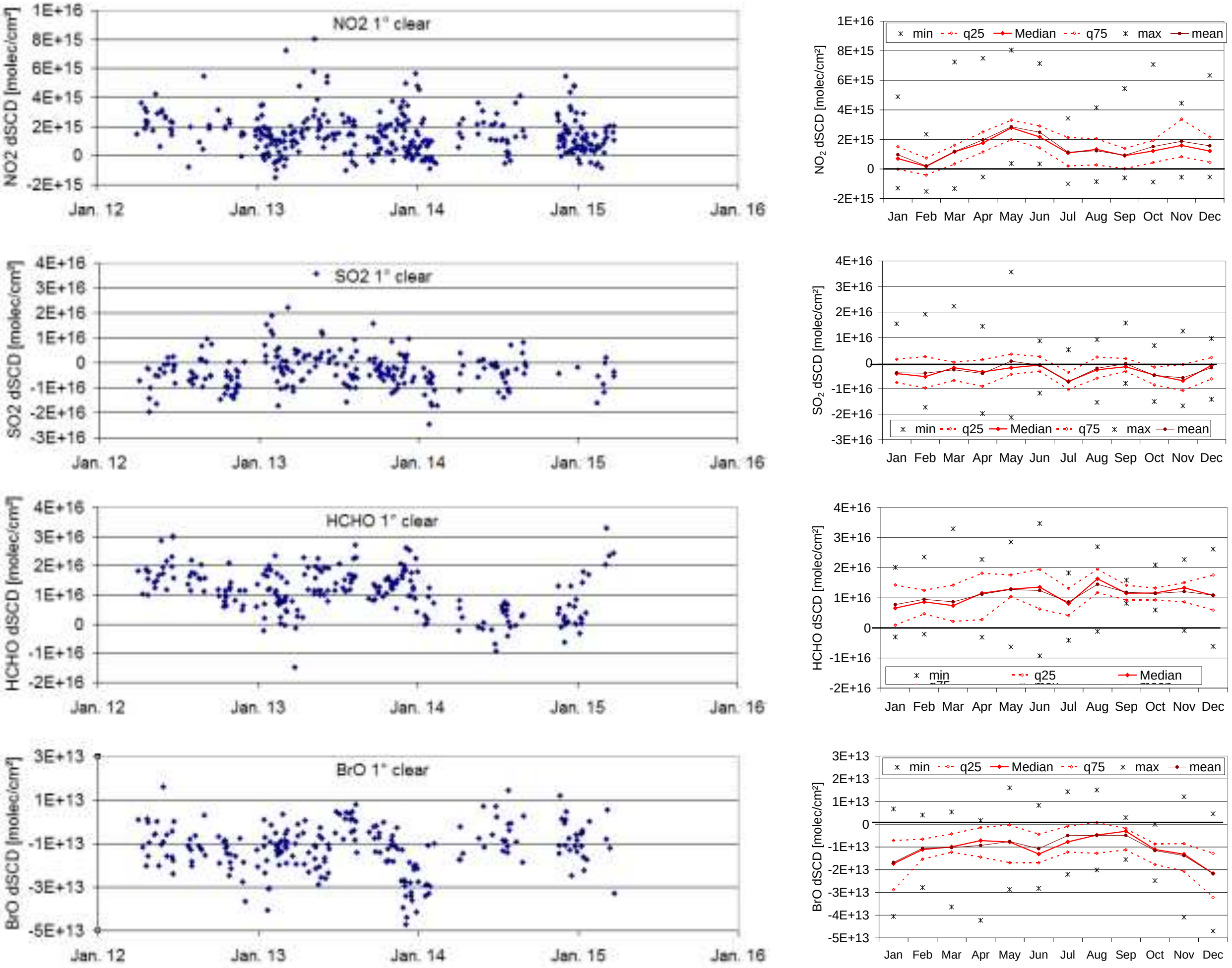

Figure 7 Left: Time series of daily averaged trace gas dSCDs at 1 °elevation for clear sky spectra and low aerosol load from 2012 to 2015, with 'Jan 12' referring to '1 Jan 2012'. **Right:** Corresponding seasonal averages.

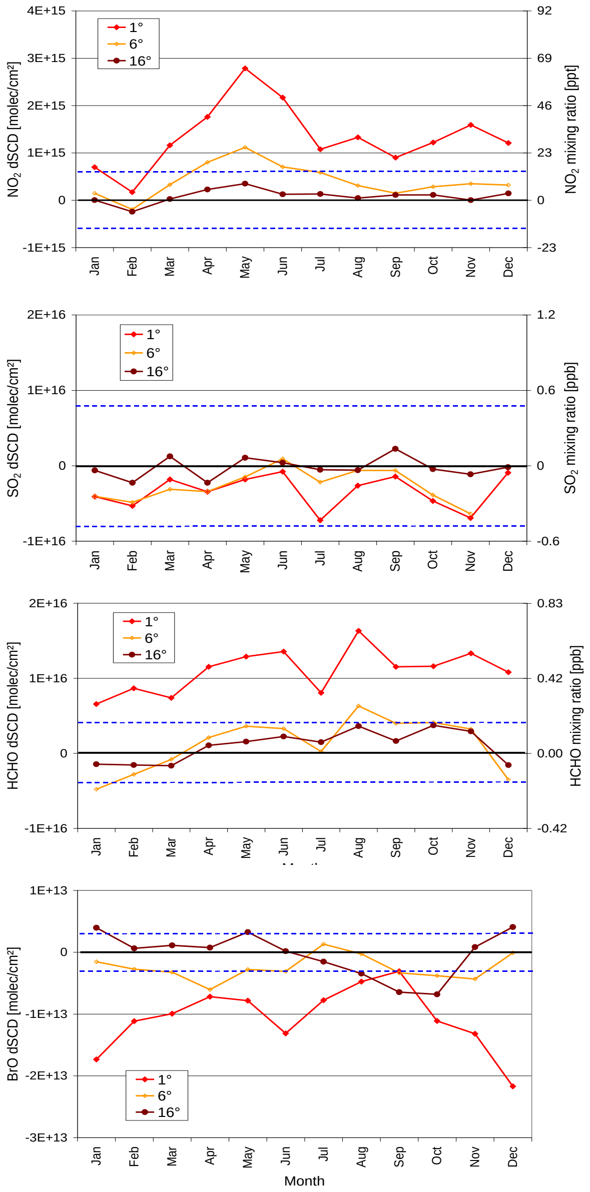

Figure 8 Seasonal means of the trace gas dSCDs for different elevation angles for clear sky and low aerosol load. For NO$_2$, SO$_2$, and HCHO the right axes represent the approximate mixing ratios for measurements at 1 ° elevation angle. The blue dotted lines indicate the systematic uncertainties, which can be considered as lower bound of the detection limit.